Research Article | Vol. 24, No. 17 | 22 Aug 2016 | OPTICS EXPRESS 19254

Optics EXPRESS

Temperature- and -roughness dependent permittivity of annealed/unannealed gold films

PO-TING SHEN,[1] YONATAN SIVAN,[2] CHENG-WEI LIN,[3] HSIANG-LIN LIU,[3] CHIH-WEI CHANG,[4] AND SHI-WEI CHU[1,5,*]

[1]*Department of Physics, National Taiwan University, 1, Sec. 4, Roosevelt Road, Taipei 10617, Taiwan*
[2]*Unit of Electrooptics Engineering, Faculty of Engineering Sciences, Ben-Gurion University of the Negev, P.O. Box 653, Be'er Sheva 8410501, Israel*
[3]*Department of Physics, National Taiwan Normal University, 162, Sec. 1, Heping E. Rd, Taipei, Taiwan*
[4]*Center for Condensed Matter Sciences, National Taiwan University, Taipei 10617, Taiwan*
[5]*NTU Molecular Imaging Center, 81, Changxing St., Taipei 10672, Taiwan*
[*]*swchu@phys.ntu.edu.tw*

Abstract: Intrinsic absorption and subsequent heat generation have long been issues for metal-based plasmonics. Recently, thermo-plasmonics, which takes the advantage of such a thermal effect, is emerging as an important branch of plasmonics. However, although significant temperature increase is involved, characterization of metal permittivity at different temperatures and corresponding thermo-derivative are lacking. Here we measure gold permittivity from 300K to 570K, which the latter is enough for gold annealing. More than one order difference in thermo-derivative is revealed between annealed and unannealed films, resulting in a large variation of plasmonic properties. In addition, an unusual increase of imaginary permittivity after annealing is found. Both these effects can be attributed to the increased surface roughness incurred by annealing. Our results are valuable for characterizing extensively used unannealed nanoparticles, or annealed nanostructures, as building blocks in future thermo-nano-plasmonic systems.

OCIS codes: (250.5403) Plasmonics; (120.6810) Thermal effects; (120.2130) Ellipsometry and polarimetry.

References and links

1. W. L. Barnes, "Metallic metamaterials and plasmonics," Philos Trans A Math Phys Eng Sci **369**(1950), 3431–3433 (2011).
2. V. M. Shalaev, "Optical negative-index metamaterials," Nat. Photonics **1**(1), 41–48 (2007).
3. A. O. Govorov and H. H. Richardson, "Generating heat with metal nanoparticles," Opt. Express **2**, 30–38 (2007).
4. V. P. Zharov and D. O. Lapotko, "Photothermal imaging of nanoparticles and cells," IEEE J. Sel. Top. Quantum Electron. **11**(4), 733–751 (2005).
5. X. Huang, P. K. Jain, I. H. El-Sayed, and M. A. El-Sayed, "Plasmonic photothermal therapy (PPTT) using gold nanoparticles," Lasers Med. Sci. **23**(3), 217–228 (2008).
6. Y. Sonnefraud, H. G. Sinclair, Y. Sivan, M. R. Foreman, C. W. Dunsby, M. A. A. Neil, P. M. French, and S. A. Maier, "Experimental proof of concept of nanoparticle-assisted STED," Nano Lett. **14**(8), 4449–4453 (2014).
7. S.-W. Chu, H.-Y. Wu, Y.-T. Huang, T.-Y. Su, H. Lee, Y. Yonemaru, M. Yamanaka, R. Oketani, S. Kawata, S. Shoji, and K. Fujita, "Saturation and reverse saturation of scattering in a single plasmonic nanoparticle," ACS Photonics **1**(1), 32–37 (2014).
8. S. Molesky, C. J. Dewalt, and Z. Jacob, "High temperature epsilon-near-zero and epsilon-near-pole metamaterial emitters for thermophotovoltaics," Opt. Express **21**(S1), A96–A110 (2013).
9. C. Clavero, "Plasmon-induced hot-electron generation at nanoparticle/metal-oxide interfaces for photovoltaic and photocatalytic devices," Nat. Photonics **8**(2), 95–103 (2014).
10. Z. Fang, Y. R. Zhen, O. Neumann, A. Polman, F. J. García de Abajo, P. Nordlander, and N. J. Halas, "Evolution of light-induced vapor generation at a liquid-immersed metallic nanoparticle," Nano Lett. **13**(4), 1736–1742 (2013).
11. X. Chen, A. Munjiza, K. Zhang, and D. Wen, "Molecular dynamics simulation of heat transfer from a gold nanoparticle to a water pool," J. Phys. Chem. C **118**(2), 1285–1293 (2014).
12. D. Kraemer, B. Poudel, H.-P. Feng, J. C. Caylor, B. Yu, X. Yan, Y. Ma, X. Wang, D. Wang, A. Muto, K. McEnaney, M. Chiesa, Z. Ren, and G. Chen, "High-performance flat-panel solar thermoelectric generators with high thermal concentration," Nat. Mater. **10**(7), 532–538 (2011).
13. D. A. Boyd, L. Greengard, M. Brongersma, M. Y. El-Naggar, and D. G. Goodwin, "Plasmon-assisted chemical vapor deposition," Nano Lett. **6**(11), 2592–2597 (2006).

#266938 http://dx.doi.org/10.1364/OE.24.019254
Journal © 2016 Received 31 May 2016; revised 29 Jul 2016; accepted 2 Aug 2016; published 10 Aug 2016

Optics EXPRESS

14. N. Zhou, X. F. Xu, A. T. Hammack, B. C. Stipe, K. Z. Gao, W. Scholz, and E. C. Gage, "Plasmonic near-field transducer for heat-assisted magnetic recording," Nanophotonics **3**(3), 141–155 (2014).
15. U. Guler, A. Boltasseva, and V. M. Shalaev, "Refractory plasmonics," Science **344**(6181), 263–264 (2014).
16. G. P. Pells and M. Shiga, "The optical properties of copper and gold as a function of temperature," J. Phys. Chem. **2**, 1835 (1969).
17. P. B. Johnson and R. W. Christy, "Optical constants of noble metals," Phys. Rev. B **6**(12), 4370–4379 (1972).
18. O. A. Yeshchenko, I. S. Bondarchuk, V. S. Gurin, I. M. Dmitruk, and A. V. Kotko, "Temperature dependence of the surface plasmon resonance in gold nanoparticles," Surf. Sci. **608**, 275–281 (2013).
19. R. B. Wilson, B. A. Apgar, L. W. Martin, and D. G. Cahill, "Thermoreflectance of metal transducers for optical pump-probe studies of thermal properties," Opt. Express **20**(27), 28829–28838 (2012).
20. Y. J. Chen, M. C. Lee, and C. M. Wang, "Dielectric function dependence on temperature for Au and Ag," Jpn. J. Appl. Phys. **53**(8S2), 08MG02 (2014).
21. A. Trügler, J.-C. Tinguely, G. Jakopic, U. Hohenester, J. R. Krenn, and A. Hohenau, "Near-field and SERS enhancement from rough plasmonic nanoparticles," Phys. Rev. B **89**(16), 165409 (2014).
22. M. Bosman, L. Zhang, H. Duan, S. F. Tan, C. A. Nijhuis, C. W. Qiu, and J. K. W. Yang, "Encapsulated annealing: enhancing the plasmon quality factor in lithographically-defined nanostructures," Sci. Rep. **4**, 5537 (2014).
23. V. Švorčík, J. Siegel, P. Šutta, J. Mistrík, P. Janíček, P. Worsch, and Z. Kolská, "Annealing of gold nanostructures sputtered on glass substrate," Appl. Phys., A Mater. Sci. Process. **102**(3), 605–610 (2011).
24. A. D. Rakić, A. B. Djurišić, J. M. Elazar, and M. L. Majewski, "Optical properties of metallic films for vertical-cavity optoelectronic devices," Appl. Opt. **37**(22), 5271–5283 (1998).
25. M. Guerrisi, R. Rosei, and P. Winsemius, "Splitting of the interband absorption edge in Au," Phys. Rev. B **12**(2), 557–563 (1975).
26. F. Hache, D. Ricard, C. Flytzanis, and U. Kreibig, "The optical Kerr effect in small metal particles and metal colloids: the case of gold," Appl. Phys., A Mater. Sci. Process. **47**, 347–357 (1988).
27. N. E. Christensen and B. O. Seraphin, "Relativistic band calculation and the optical properties of gold," Solid State Commun. **8**(15), 1221–1226 (1970).
28. A. Marini, M. Conforti, G. D. Valle, H. W. Lee, X. T. Tr, W. Chang, M. A. Schmidt, S. Longhi, P. S. J. Russell, and F. Biancalana, "Ultrafast nonlinear dynamics of surface plasmon polaritons in gold nanowires due to the intrinsic nonlinearity of metals," New J. Phys. **15**(1), 013033 (2013).
29. H. R. Moon, D.-W. Lim, and M. P. Suh, "Fabrication of metal nanoparticles in metal-organic frameworks," Chem. Soc. Rev. **42**(4), 1807–1824 (2013).
30. C. Liu, C. C. Mi, and B. Q. Li, "The plasmon resonance of a multilayered gold nanoshell and its potential bioapplications," IEEE Trans. NanoTechnol. **10**(4), 797–805 (2011).
31. S. W. Chu, T. Y. Su, R. Oketani, Y. T. Huang, H. Y. Wu, Y. Yonemaru, M. Yamanaka, H. Lee, G. Y. Zhuo, M. Y. Lee, S. Kawata, and K. Fujita, "Measurement of a saturated emission of optical radiation from gold nanoparticles: application to an ultrahigh resolution microscope," Phys. Rev. Lett. **112**(1), 017402 (2014).
32. Y. Sivan and S.-W. Chu, "Nonlinear plasmonics at high temperatures," Nanophotonics (accepted).
33. R. L. Olmon, B. Slovick, T. W. Johnson, D. Shelton, S.-H. Oh, G. D. Boreman, and M. B. Raschke, "Optical dielectric function of gold," Phys. Rev. B **86**(23), 235147 (2012).
34. H. Reddy, U. Guler, A. V. Kildishev, A. Boltasseva, and V. M. Shalaev, "Temperature-dependent optical properties of gold thin films," https://arxiv.org/abs/1604.00064.
35. C. F. Bohren and D. R. Huffman, *Absorption and Scattering of Light by Small Particles* (Wiley-VCH Verlag GmbH, 2007).
36. J. W. C. Vries, "Resistivity of thin Au films as a function of grain diameter and temperature," J. Phys. F **17**(9), 1945–1952 (1987).
37. D. Lepage, D. Carrier, A. Jiménez, J. Beauvais, and J. J. Dubowski, "Plasmonic propagations distances for interferometric surface plasmon resonance biosensing," Nanoscale Res. Lett. **6**(1), 388 (2011).
38. S. Babar and J. H. Weaver, "Optical constants of Cu, Ag, and Au revisited," Appl. Opt. **54**(3), 477–481 (2015).
39. K. M. McPeak, S. V. Jayanti, S. J. P. Kress, S. Meyer, S. Iotti, A. Rossinelli, and D. J. Norris, "Plasmonic Films Can Easily Be Better: Rules and Recipes," ACS Photonics **2**(3), 326–333 (2015).

1. Introduction

Plasmonics has emerged to be one of the most important branches in photonics, due to its potential in greatly enhanced light-matter interaction within nano-scale structures [1,2]. In the early stage of development, the inherent absorption in the metal was thought to be a substantial obstacle towards real-life applications. However, in recent years the applied plasmonic researches exploit the absorption as means to generate heat on the nanoscale [3]. The temperature scale of this new sub-field, thermo-plasmonics, starts from photothermal imaging [4], through cancer treatment [5], super-resolution microscopy [4,6,7], plasmonic photovoltaics [8,9], water boiling, and super-heating [1,10,11], up to thermo-photovoltaics [8], solar thermo-electric generators [12], plasmon-mediated photocatalysis [9], plasmon-

Optics EXPRESS

assisted chemical vapor deposition [13] and heat-assisted magnetic recording [14], which may involve temperatures higher than 2000K [15].

Such studies obviously require knowledge of temperature-dependent metal permittivity. However, it turns out that experimental measurements of such dependencies are rather scarce and there is no complete and correlated set of data from room temperature up to the melting temperature. For example, the old data of [16], extracted from spectroscopic data of a heated gold film (295 - 770K), specifies the absorbance (from which the imaginary part of the permittivity can be extracted), but not the real part of the permittivity. Compared to the well-recognized data of [17], the absorbance value in the former study is rather high, possibly due to high surface roughness in their samples.

In a recent study [18], the temperature dependence of absorption from gold nanospheres in silica was measured. Although detailed extinction spectra is shown over the widest temperature range studied so far (up to ~1200K), their results cannot unambiguously extract the real and imaginary parts of the gold permittivity, critical to study other geometries.

To date, the most systematic study of the temperature dependence of gold permittivity was performed in two recent works [19,20]. However, instead of showing the values of the permittivity itself, only values of the thermo-derivative were provided in [19]. Moreover, a rather rough estimate of the thermo-derivative was provided, based on only two temperatures (300 and 430K). On the other hand, better temperature resolution is provided in [20], but only for a narrow spectral range (700-900nm) and temperatures beyond the boiling point. No *in situ* analysis of annealing effects was considered.

It is well known that increasing temperature induces changes in the morphology of gold due to annealing. Surprisingly, no morphological information was included in previous temperature dependent permittivity studies. Although an irregularly small thermo-derivative is observed at 460K in [20], no discussion about annealing was given. It is known that annealing significantly affects plasmonic effects [21,22]. However, since most plasmonic nanostructures are fabricated without annealing, it is critical to examine the variation of fundamental physical property of gold before and after annealing.

In this work, *in situ* temperature dependent permittivity of gold before and after annealing was studied from room temperature to annealing temperature, with 10K steps. We found more than one order difference in the thermo-derivatives, for the first time to our knowledge. In addition, we found an interesting anomaly that the imaginary permittivity of gold film increases after annealing, possibly due to the non-specular reflection from the surface roughness. Our work will serve as a valuable reference to characterize gold nanophotonic devices.

2. Experimental setup

The gold film was made by electron beam evaporation of gold with 99.99% purity onto a silicon nitride substrate with 5nm titanium as an adhesion layer. Its thickness is 130 ± 16 nm, which should be enough to be treated as bulk [23]. For unannealed sample, the deposited film is directly used. For annealed sample, the gold film is placed at 600K for 15 minutes, under 10^{-3} atm, and then cooled off to 300K. The temperature dependent permittivity is acquired with a spectroscopic ellipsometer (M2000 U, J.A. Woollam Co, NE) from 190 to 1600 nm. The conductivities of the gold films are measured by four terminal sensing on a ceramic chip holder. The surface roughness and profile of gold films before and after annealing are measured with an atomic force microscope (XE-100, Park Systems, Korea).

3. Results

3.1 Permittivity at room temperature

Figures 1(a) and 1(b) show the real part and imaginary part of gold permittivity measured at 300K. The ellipsometry data from annealed and unannealed films are plotted as red and blue

Optics EXPRESS

lines, respectively. Scanning electron microscope images of the gold films before and after annealing are separately shown in Figs. 1(c) and 1(d). Obviously, the grain size greatly increases in Fig. 1(d), manifesting the effect of annealing.

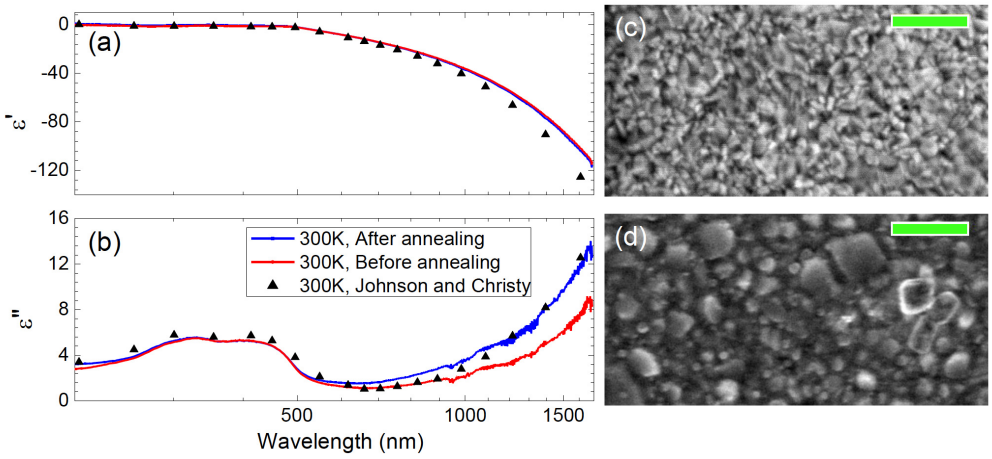

Fig. 1. Gold permittivity at room temperature before and after annealing: (a) the real part ε' and (b) the imaginary part ε". Significant variation in the imaginary part is found after annealing. (c) and (d) are SEM images before and after annealing, respectively. Scale bar: 400nm. The grain sizes are much larger after annealing.

Our permittivity results are in good agreement with the generally recognized work of [17], shown as green dashed lines. Interestingly, in the visible range, the permittivity (both real and imaginary) is not affected significantly by annealing. In the near-infrared region above 1000 nm, slight deviations, in both real and imaginary parts, are found between our data and [17] before annealing. For the real part, annealing does not affect the correspondence much, but for the imaginary part, after annealing, it becomes well-matched to [17] again.

3.2 Temperature-dependent permittivity of unannealed gold

By increasing temperature gradually on the unannealed film, remarkable variations of gold permittivity at several wavelengths throughout the spectral range are observed, as shown in Fig. 2. For the real part in Fig. 2(a), the data below 520nm exhibits only small variation. The variations are more and more significant for increasing wavelength, but all exhibit the same trend of decrease and then increase above 450K, reflecting the onset of annealing effect. On the other hand, for the imaginary part in Fig. 2(b), monotonic increase is observed for wavelengths above 520 nm; while for 405nm, the trend is increase and then decrease above 450K. The largest variation is found at 1200nm, whose imaginary permittivity increases by 133% from 300 to 570K.

To highlight the variation trend, real and imaginary parts of thermo-derivatives are given in Figs. 2(c) and 2(d), respectively. The real parts are negative at all wavelengths at low temperatures, but become positive above 450K, with a peak at ~500K. For the imaginary parts, all decrease from positive at low temperature, and revert above 450K. Only wavelength below 520nm exhibits negative derivative at high temperatures. By dividing the thermo-derivatives to the permittivities, the relative change of imaginary part is much larger than real part.

Optics EXPRESS

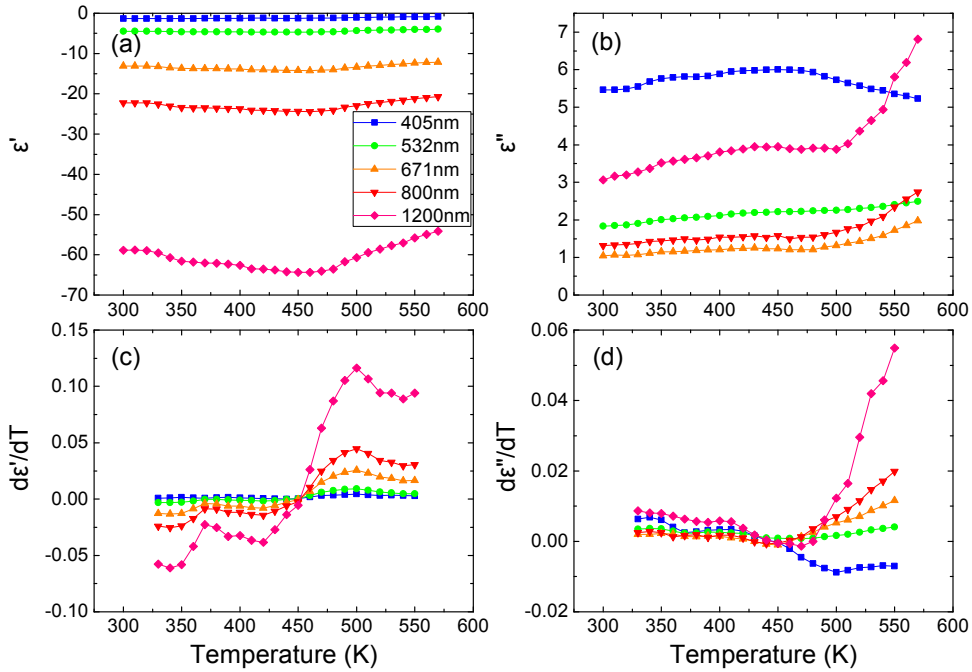

Fig. 2. Temperature-dependent permittivity at selected wavelengths with annealed gold films: (a) the real part ε' and (b) the imaginary part ε". (c) and (d) are the corresponding thermo-derivatives of ε' and ε", respectively. For both real and imaginary parts, the thermo-derivatives are larger for longer wavelengths, and increase quickly above 450K.

3.3 Temperature-dependent permittivity of annealed gold

Figures 3(a) and 3(b) show the permittivity of the annealed gold film with increasing temperature. Compared to Fig. 2, the variation is much smaller and smoother. For both the real and imaginary parts in the visible band, linear trends are observed below 450K, justifying the result in [19]. In Fig. 3(a), for 405nm, the overall permittivity variation is 12%; while for the rest wavelengths above 520nm, the permittivity variations are less than 5%. On the other hand, in Fig. 3(b), for 405nm, the permittivity variation is less than 6%; for other wavelengths, the variations are in the range of 20 - 40%, much smaller than the unannealed film.

The corresponding thermo-derivatives of real and imaginary parts are drawn in Figs. 3(c) and 3(d), respectively. Except 405 nm, all wavelengths exhibit similar trends. The real parts decrease at low temperature, and start to increase above 500K. The imaginary parts are positive and increase monotonically. Comparing to Figs. 2(c) and 2(d), the thermo-derivatives of the annealed film are nearly one order smaller than the unannealed film.

Optics EXPRESS

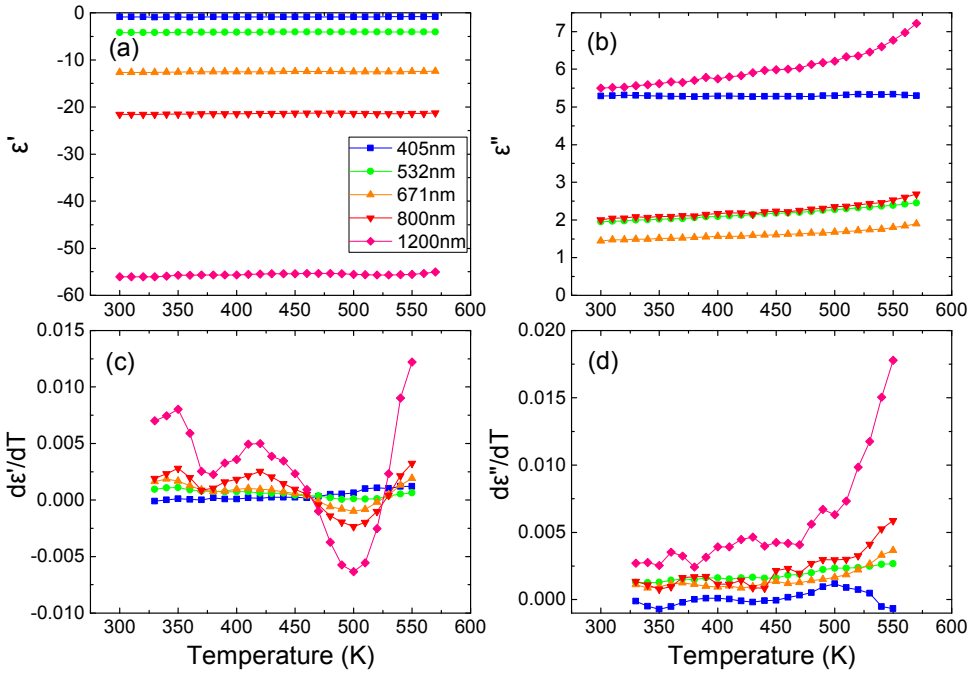

Fig. 3. Temperature-dependent permittivity at selected wavelengths with annealed gold films: (a) the real part ε' and (b) the imaginary part ε". (c) and (d) are the corresponding thermo-derivatives of ε' and ε", respectively. Similar to Fig. 2, for both real and imaginary parts, the thermo-derivatives are larger for longer wavelengths, and increase quickly above 500K. However, different from Fig. 2, the thermo-derivatives are much smaller in the annealed film.

3.4 Temperature-dependent parameters of Lorentz Drude model

To be more quantitative and to facilitate future thermo-plasmonic studies, Lorentz-Drude fitting is performed at different temperatures. The complex permittivity is expressed as

$$\varepsilon(\omega) = \varepsilon_{intra}(\omega) + \varepsilon_{inter}(\omega) \tag{1}$$

The first term is the contribution from intraband free-electron transition, corresponding to the Drude model, which is

$$\varepsilon_{intra}(\omega) = \varepsilon_{\infty} - \frac{\omega_p^{\,2}}{\omega^2 + i\omega\Gamma_D} \tag{2}$$

where ε_{∞} is the high frequency permittivity, ω_p is the plasma frequency, and Γ_D is the damping constant of free electron response. The second term in Eq. (1) is the interband contribution, described by the summation of Lorentz terms, and can be written as

$$\varepsilon_{inter}(\omega) = \omega_p^{\,2} \sum_{m=1}^{k} \frac{f_m}{\omega_m^2 - \omega^2 - i\omega\Gamma_m} \tag{3}$$

where m is the number of oscillators with frequency ω_m, oscillator strength f_m, and damping constant Γ_m. According to [24–27], five oscillators at 4.3, 3.5, 2.97, 2.3, and 1.7eV are considered here. The fitting results are shown in Fig. 4 and in Table 1, where three different temperatures are selected: 300K, 450K (onset of annealing), and 570K. The fitting is reasonably well for the whole wavelength range in our ellipsometry measurement.

Optics EXPRESS

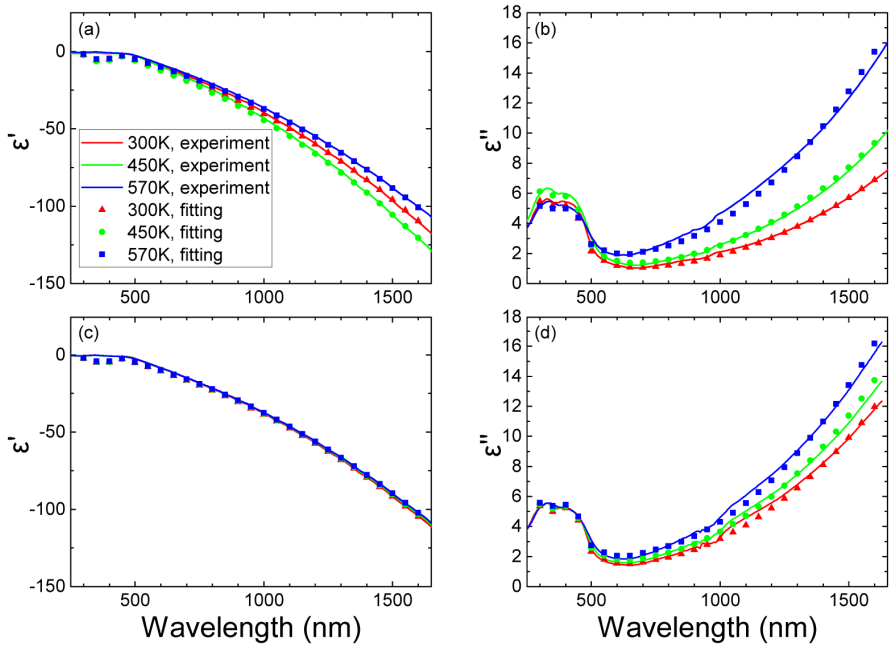

Fig. 4. The Lorentz-Drude fitting (symbols) compared to experimental result (lines). (a) the real part ε' and (b) the imaginary part ε" with the unannealed film; (c) the real part ε', and (d) the imaginary part ε" with the annealed film.

Table 1. Temperature Dependent Lorentz Drude Parameters of Gold

	Unannealed			Annealed		
Temperature (K)	300	450	570	300	450	570
ε_∞	1.00	1.15	1.35	1.03	1.24	1.3
ω_p (eV)	8.22	8.63	8.023	8.12	8.072	8.023
Γ_D (eV)	0.046	0.057	0.113	0.086	0.099	0.117
ω_1 (eV)		4.3			4.3	
f_1	0.29	0.29	0.293	0.33	0.36	0.38
Γ_1 (eV)	0.8	0.805	0.81	1	1.05	1.1
ω_2 (eV)		3.5			3.5	
f_2	0.0244	0.0242	0.0244	0.019	0.0199	0.0207
Γ_2 (eV)	0.1	0.105	0.11	0.1	0.105	0.11
ω_3 (eV)		2.97			2.97	
f_3	0.151	0.148	0.146	0.128	0.13	0.132
Γ_3 (eV)	0.6	0.605	0.61	0.6	0.605	0.61
ω_4 (eV)		2.3			2.3	
f_4	0.0035	0.0095	0.015	0.0048	0.0072	0.012
Γ_4 (eV)	0.5	0.75	0.8	0.5	0.6	0.7
ω_5 (eV)		1.7			1.7	
f_5	0.0002	0.0011	0.0024	0.0012	0.0018	0.00305
Γ_5 (eV)	0.4	0.45	0.5	0.4	0.45	0.5

Optics EXPRESS

In the fitting process, we start from considering the intraband contribution, as well as the two interband oscillators at 2.3 and 1.7 eV. From [25] and [28], the contribution of the 2.3eV oscillator to thermo-modulations of the imaginary permittivity should dominate that of the 1.7eV one, as indeed is seen in Table 1. Since the main variation occurs in the infrared regime, where intraband oscillator dominates, the temperature-dependent variation of the Drude damping constant Γ_D is the largest. An interesting note is that although the oscillator strengths at 2.3eV and 1.7eV are very small, they are required to fit the permittivity well in the green-red spectral region.

Then, the rest high-energy oscillators (4.3, 3.5, 2.97eV) are added to fit the spectrum in the ultraviolet-blue range. Although the oscillator strengths of these high-energy oscillators are larger than the low-energy ones (2.3 and 1.7eV), their temperature dependence of Γ is much lower, in agreement with [27].

4. Discussion

In this work, we find not only the room-temperature permittivity of the unannealed film is different from the annealed film, but also the thermo-derivative is much larger. Since most metallic nanoparticles are fabricated in solutions [29], they are in nature multi-crystalline, i.e. unannealed. It is apparently critical to use correct permittivity data for plasmonic calculations.

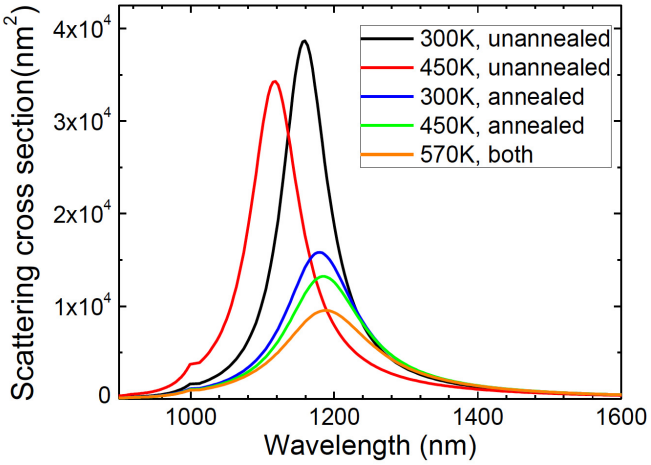

Fig. 5. Temperature/annealing dependency of scattering cross section spectrum with a 5nm gold shell on a 50nm diamond core. Since the permittivity of unannealed and annealed gold at 570K are very similar to each other, only one line is given at 570K. The plot manifests the importance of annealing effect on the permittivity.

To highlight this dependence, Fig. 5 shows the calculated scattering cross section from a gold nanoshell, resonant near 1200 nm in the biological transparent window [30]. More than 150% difference is found between the annealed and unannealed spectra at 300K. It is even more dramatically to consider the temperature dependent resonance. Comparing between 300K and 570K lines in Fig. 5, the unannealed particle exhibits more than 400% variation of scattering cross section, while the annealed one has less than two-fold variation in this temperature range. Other than cross section variation, the spectral resonance of the unannealed particle shows blue shift from 300K to 450K, and then red shift from 450K to 570K, corresponding to the temperature dependence of the real part of the permittivity in Fig. 2. Based on our finding, the factor of temperature-dependent permittivity and annealing need to be included in future thermo-plasmonic studies. Specifically, this data already proved useful in reproducing the experimental results of [30] by numerical simulations [31].

It is interesting to note an unusual phenomenon in Fig. 1(b): higher imaginary permittivity after annealing. The conventional concept is that annealing creates larger grains, reducing

Optics EXPRESS

boundary areas, resulting in lower absorption and thus, lower imaginary permittivity is expected. To offer some physical insight into this unusual phenomenon, we first measure DC conductivity of the film before and after annealing. We found that the film conductivity increases by 10% after annealing, implying that the free electron damping rate Γ_D, as well as the imaginary part of the permittivity ε" is reduced at zero frequency. The result is in good agreement with conventional knowledge [35]. Therefore, it is not the electron damping, but the microscopic optical effects from the grains on the deposited film that should account for the unusual increase of imaginary permittivity.

Two recent studies [32,33] that compared morphology versus permittivity also find larger imaginary permittivity from a gold film with larger grains. To explain this phenomenon, we point out that in an ellipsometer, specular reflection is collected. The reduction of the specular reflection is equivalent to increase in loss, and in turn is interpreted as a larger of ε". There are several possible microscopic optical mechanisms that may induce reduction of specular reflection on the annealed gold film. By considering the granular structure of the film, it can be viewed as a random grating. The first possibility is, apparently, non-specular reflection from the grating, reducing light intensity in the specular reflection. The second possibility is enhanced forward scattering, i.e. Mie scattering, due to the larger grains observed after annealing [34], so the specular reflection also decreases. However, this factor would be less important if the film is optically thick. The third possibility is coupling of incoming light to surface plasmon polaritons (SPP) by the random grating, but this is likely to be much weaker since our grain size, and corresponding "grating period", exceeds substantially the momentum mismatch between incoming photon and SPP.

To provide further verification on the possible micro-optical mechanisms, surface profiles of the film before and after annealing are characterized by atomic force microscopy (AFM), as shown in Fig. 6. After annealing, grain size (i.e., horizontal inhomogeneity) and surface roughness (height inhomogeneity) increase together, both helpful to enhance the random grating effect. To exclude the possibility of Mie scattering, we note that the mean roughness increases from 2.6nm to 4.5nm after annealing. Considering the average film thickness to be 130 nm, the AFM result confirms the film to be optically thick, so Mie scattering is not dominant. The increased roughness still cannot allow for efficient SPP coupling [36]. Therefore, we suggest that the non-specular reflection of the random grating structure on the annealed film is the underlying optical mechanism responsible for the additional loss in ellipsometry measurement.

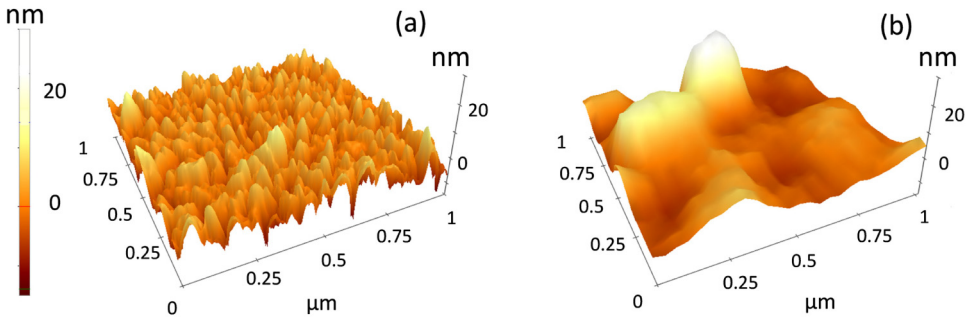

Fig. 6. AFM profiles for (a) unannealed (b) annealed gold film. The gold grains aggregated after annealing, creating grating-like structures.

Having said this, one should appreciate that the differences in the temperature dependence of the permittivity of unannealed and annealed films should primarily be attributed to the modified morphology rather than to intrinsic bulk properties of gold [33]. Nevertheless, it is surprising that our imaginary permittivity of the annealed film fits well with [17], which has been cited over 10,000 times and whose films were annealed at 423K for 9 hours. The low-

Optics EXPRESS

temperature and long annealing should in principle create a uniformly annealed film. However, since no morphological information was provided in [17], we suspect that their result, in fact, represents large gold grains, i.e. partially annealed gold. To further justify this point, two recent reports [37,38] with high-quality films showed smaller imaginary permittivity than results from [17].

A final remark is on the adhesion layer. During our sample deposition, a titanium layer facilitated the adhesion of gold, and thus improved the overall film flatness. Nevertheless, when annealing the film, the adhesion force from titanium might cause gold to form large grains. In terms of the thermo-derivative, titanium should not dominate the response. Compared to [20], where a Cr adhesion layer is used, the resulting thermo-derivative of gold is very similar to our result, manifesting the insignificant role of the adhesion layer.

5. Conclusion

Since plasmonic properties are dominated by metal permittivity, which is highly dependent on temperature and crystalline structure, here we provide detailed characterization of thermo-derivatives of annealed and unannealed gold, and detailed temperature-dependent Lorentz-Drude parameters, for the first time. Substantial variations of permittivity, especially the imaginary part, are found. An unusual increase of imaginary permittivity after annealing was observed, and can be attributed to scattering/diffraction from random grating effect of the large grains on the annealed film. Conventionally, permittivity of annealed gold is adopted to calculate plasmonic responses. However, since most plasmonic nanostructures are fabricated with unannealed metal, corresponding unannealed permittivity should be adopted, resulting in very different plasmonic resonance strength. Our work points out not only the missing consideration for permittivity measurement, but also the significance of choosing correct set of permittivity for future thermo-nano-plasmonic studies.

Funding

This work was supported by the National Science Council of Taiwan under contract No. NSC-102-2112-M-002-018-MY3 and NSC-105-2628-M-002-010-MY4.

Acknowledgments

The authors thank Ms. Pin-Yi Li for her assistance with the measurement of conductivity; Ms. Yen-Ting Wang and Dr. Woei-Wu Pai for the AFM acquisition; Mr. Hsiao-Wen Chen for his assistance in ellipsometry. SWC acknowledge the generous support from the Foundation for the Advancement of Outstanding Scholarship.